



## An experimental-computational framework for validating *in-vivo* ECG inverse algorithms

M.P. Nash\*, C.P. Bradley\*, L.K. Cheng\*\*, A.J. Pullan\*\* and D.J. Paterson\*

\* University Laboratory of Physiology, Parks Road, Oxford OX1 3PT, United Kingdom.

\*\* Department of Engineering Science, The University of Auckland, New Zealand.

[martyn.nash@physiol.ox.ac.uk](mailto:martyn.nash@physiol.ox.ac.uk)  
[chris.bradley@physiol.ox.ac.uk](mailto:chris.bradley@physiol.ox.ac.uk)

### Abstract:

We aimed to correlate the electrical signals from a dense sampling of *in-vivo* body surface ECGs (256 unipolar recording sites, approximately 15 mm spacing) with concurrent electrical activity recorded directly from the ventricles (127 epicardial electrodes, approximately 5-10 mm spacing) in a closed-chest anaesthetised pig. Simultaneous ventricular epicardial and body surface electropotential mapping (2 kHz sampling rate) was performed during (i) normal sinus rhythm; (ii) posterior epicardial pacing; and (iii) apical epicardial pacing. Torso and epicardial electrode locations (most of which were obtained using a mechanical digitiser) were projected onto customised 3D anatomico-computational models of the porcine torso and heart, which were used to interpret the body surface potential field and the epicardial activation sequence, respectively. The physiological changes in ventricular activity were clearly reflected in alterations to the body surface potential maps during all interventions. The techniques and data presented here form the basis of an integrated experimental and computational framework we have developed to assess the accuracy of numerical approaches to inverse electrocardiography.

**Keywords:** Cardiac activation sequence, body surface potential mapping, experimental ECG inverse validation

## Introduction

Reliable quantitative and objective assessment of regional electrocardiac function from non-invasive recordings at the body surface has been an area of extensive research by bioengineers and cardiologists for several decades. Several computational approaches that attempt to solve the electrocardiographic inverse problem have been developed, but to date their suitability for *in-vivo* and clinical situations has not been

firmly established. Before any inverse electrical imaging procedure can be used as a non-invasive diagnostic tool with confidence, it must first be validated so that recorded experimental observations can be faithfully reproduced.

The primary objective of this study was to simultaneously sample dense arrays of ventricular epicardial and body surface electropotential signals from an anaesthetised pig under control and conditions of abnormal epicardial activation. Here we present recent data, which we have recorded to investigate the effects of epicardial pacing on ventricular activation and the associated electrical activity at the body surface. These studies form part of our database of controlled interventions that we plan to use to validate and refine computational approaches to inverse electrocardiography. Of particular interest, is the recent method of Huiskamp and Greensite [1], which has been formulated in terms of the underlying cardiac activation sequence rather than epicardial electropotentials. This has significant advantages over epicardial potential formulations, not least in that it deals directly with the underlying physiological process (namely the cardiac activation sequence) responsible for generating the body surface potentials.

## Methods

### *In-vivo measurements*

Anaesthesia, surgical and electropotential mapping methods have been fully described previously [2], but brief descriptions are included here. The investigation conforms to the Guide for the Care and Use of Laboratory Animals published by the US National Institutes of Health (NIH Publication No. 85-23, revised 1996) and under a British Home Office Project License (no. PPL 30/1133).

*Anaesthesia and haemodynamic measurements:* A 29 kg domestic pig was anaesthetised with 2-3% halothane (Fluothane, ICI), for induction, and bolus infusions of alpha-chloralose (Sigma, 100 mg/kg i.v., repeated approximately every two hours as required) for maintenance. Femoral arteries and veins were cannulated and arterial blood pressure (ABP) and the Lead II ECG were monitored, while core temperature and arterial blood gases were maintained at physiological values. ABP was measured using a saline-filled pressure transducer (SensoNor 840, Norway) connected to a real time data acquisition system (MP 100, Biopac Systems Inc.) employing Acqknowledge 3.0 software for the Macintosh (Macintosh Quadra 950). Heart rate (HR) was computed using this software.

*In-vivo heart geometry:* 3D ultrasound (HPSONOS 5500) was used pre-operatively to obtain the size, orientation and location of the heart within the torso cavity. The image sets were manually digitised and segmented to provide a parametric 3D representation of the ventricular surfaces. A mechanical digitising arm (FARO Technologies Inc.) was used to record the position and orientation of the 3D ultrasound probe, in order to quantitatively register the ultrasound image sets with respect to a pre-defined anatomical frame of reference. In this way, the experimental heart geometry could be located inside the customised computational torso model (described below).

*Surgery and mapping:* The animal was tracheotomised, artificially ventilated (Oxford Mark II ventilator, Penlon), thoracotomised and pericardectomy was performed. An elasticised sock containing 127 unipolar stainless steel electrodes (inter-electrode spacing approximately 5-10 mm; Biomedical Instruments Designers, Montreal) was slipped over the ventricles. The chest was then re-closed (the epicardial electrode wires exited near the diaphragm) and filled with saline to eliminate air pockets. A custom-made elasticated vest containing 256 electrodes (inter-electrode spacing approximately 15 mm) was fitted to the animal. Electrodes on the epicardial sock and torso vest were connected to a 448 channel Unemap cardiac mapping system (Uniservices, Auckland). Body surface and epicardial unipolar electropotential signals were simultaneously recorded on demand with a 2 kHz sampling rate. All signals were referred to the Wilson's central terminal (WCT; electrical average of the signals recorded from front and left-rear limbs), whilst the right-rear limb was driven by the negative of the WCT signal ("right leg drive") to increase the signal-to-noise ratio.

*Torso electrode localisation:* We used the FARO arm to directly record the majority (approximately 85%)

of 3D locations of the torso electrodes. The remaining torso electrodes, situated on the back of the animal, could not be directly digitised, thus we interpolated their positions from the known organisation of the electrodes on the vest together with the measured positions of the nearest obtainable neighbours.

*Epicardial electrode localisation:* Perhaps the most difficult geometric information to obtain was the set of epicardial electrode locations. During initial studies, we carefully re-opened the chest following all protocols and digitised as many electrodes as possible (approximately 40-50%) using the FARO arm. The unknown epicardial electrode locations were estimated using the pre-defined electrode topography on the epicardial sock. During more recent studies, we have integrated a sonomicrometry system (Sonometrics Corporation, Canada) into our experimental setup to more accurately determine the locations of epicardial electrodes within the closed chest. This work is still in progress in our laboratory.

### Computational analysis

*Generic mathematical model of the pig torso:* We constructed an anatomically accurate generic model of the pig by first placing a pig in a CT scanner and recording a sequence of cross-sectional images. These images were manually digitised to provide 3D data sets for the endocardial, epicardial, lungs and skin (torso) surfaces. A non-linear optimisation procedure, which incorporated non-linear constraints and smoothing, was used to obtain a parametric 3D representation for each surface.  $C^1$  cubic Hermite elements were used to define the smoothly continuous anatomical geometry. Full details of the fitting procedure may be found in [3].

*Torso model customisation:* The generic torso model described above was customised to provide a computational model for each experimental animal. The customisation of each pig was achieved by using the FARO arm to locate a number of anatomical landmarks on the experimental animal and hence set up an anatomical frame of reference. The same anatomical landmarks were identified on the generic pig model and a non-linear fitting procedure, which minimises the differences between the two sets of anatomical landmarks, was used to transform the generic model into the customised model. Further details of the customisation procedure may be found in [4] and [5].

**Figure 1** illustrates the torso model customisation procedure. The generic torso mesh (beige surface) is customised into the experimental model (orange wire-frame) by minimising the differences between anatomical landmarks located on the generic model (blue spots) and on the experimental animal (red spots; red arrows show the physical translations). Torso electrode locations (orange spots) are projected (green arrows show perpendicular projections) onto the customised mesh as part of the body surface potential mapping process.



**Figure 1:**  
See text for details.

*Torso mapping:* We used the customised torso model and measured vest electrode locations to interpret the recorded body surface ECGs. First, we projected the measured 3D torso electrode locations onto customised torso model using a nearest approach technique. Secondly, we identified a single cycle of electrocardiac activity using the Unemap software and applied a 50 Hz notch filter to reduce noise. Finally, we fitted a body surface potential field for every time sample to generate an integrated 3D time-varying description of the electropotential changes at the torso surface. Body surface potential maps (BSPMs) were displayed on the customised model using a colour spectrum, where blue and red denoted -0.5 mV and +0.5 mV, respectively. The BSPM animations in the results section were created with a temporal resolution of 0.5 ms between frames (corresponding to the 2 kHz sampling rate).

*Epicardial mapping:* We used the echocardiographically derived heart model and the 3D locations of the

sock electrode to interpret the *in-vivo* epicardial surface electropotential signals. First, we fitted the known topographical organisation of sock electrodes to the epicardial surface of the heart model using similar methods to the vest electrode projection process. Secondly, we identified a single cycle of electrocardiac activity using the Unemap software (the epicardial signals did not require filtering) and determined the activation time for each electrode as the most negative electropotential slope. Finally, we fitted a spatially varying scalar field to the epicardial electrode activation times to obtain an epicardial activation sequence, which was displayed on the customised heart model, using a colour spectrum with red and blue denoting earliest and latest epicardial activation, respectively. The epicardial activation sequence animations in the results section were created with a temporal resolution of 0.5 ms between frames.

## Experimental protocols

1. *Sinus rhythm*: Simultaneous body surface potential and epicardial activation sequence mapping was performed to determine the control electrocardiographic state of the animal.
2. *Posterior epicardial pacing*: The ventricles were electrically stimulated (10 V amplitude; 2 ms pulse width; 20-30 pulses/min above baseline HR) via a sock electrode located at the posterior basal epicardial surface. During this captured external pacing, ventricular epicardial and body surface potential recordings were simultaneously sampled.
3. *Apical epicardial pacing*: The same pacing protocol was used via a sock electrode located at the anterior apical epicardial surface, while simultaneously sampling ventricular epicardial and body surface potentials.

## Results

### Sinus rhythm

Under control conditions, epicardial activation (illustrated in Figure 2a) progressed about the ventricles from mid-anterior portions to posterior-basal tissue in just 20 ms. This apparently rapid spread of epicardial activation was likely to be due to a primarily transmural wave of propagation (typical of normal ventricular excitation) and is illustrated in the [animated activation sequence](#), which uses red and blue to represent resting and depolarised tissue, respectively. Several activation breakthrough zones were observed and were likely to be due to the varying thickness of the ventricular walls. The corresponding BSPM (at peak R) is shown in Figure 2b and the [temporally animated BSPM](#) shows the electropotential changes that occurred as the wave of excitation propagated throughout the heart (frames are separated by 0.5 ms).

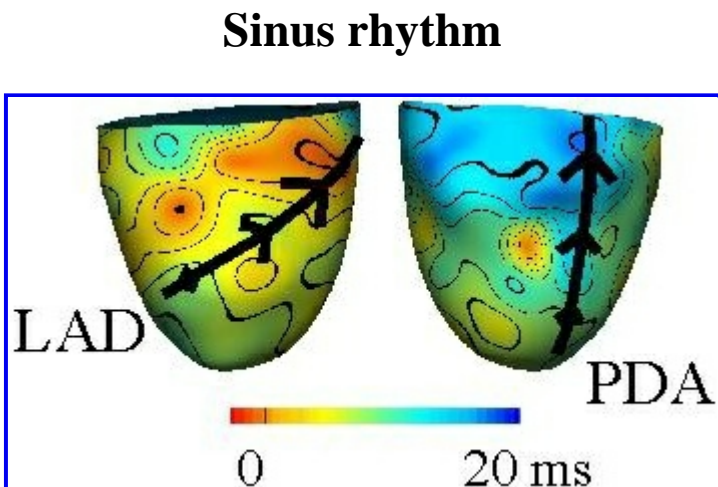


**Figure 2a:** Ventricular epicardial activation map illustrated from anterior (left) and posterior (right) viewpoints. Zones of earliest epicardial activation (red) are separated from latest activation regions (blue) by isochronal contours (black bands). LAD and PDA denote left anterior and posterior descending coronary arteries, respectively (thick black lines).

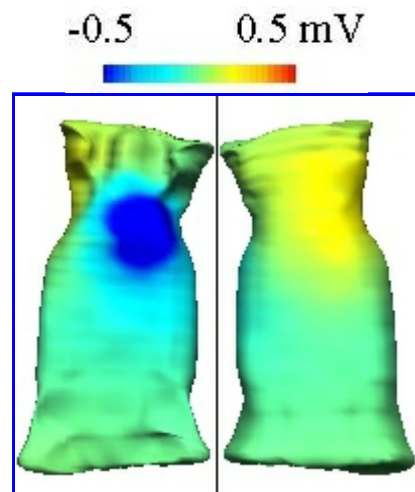


**Figure 2b:** Body surface potential map at peak R viewed from the chest (left) and the back (right). The neck is located at the top and tail at the bottom. (Click for animated version.)

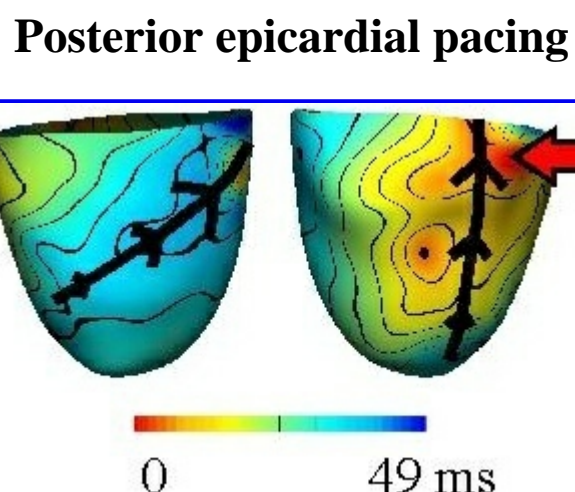


**Figure 3a:** The pacing site is represented by the red arrow. See Figure 2a legend and text for details.

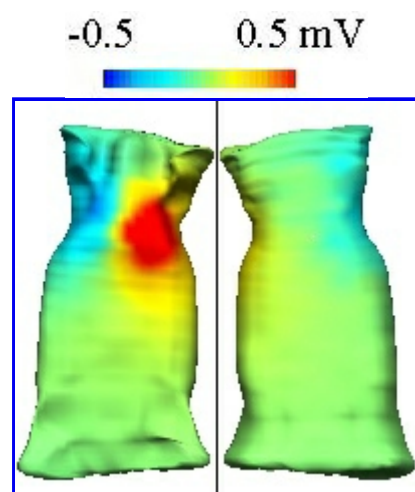


**Figure 3b:** See Figure 2b legend and text for details.

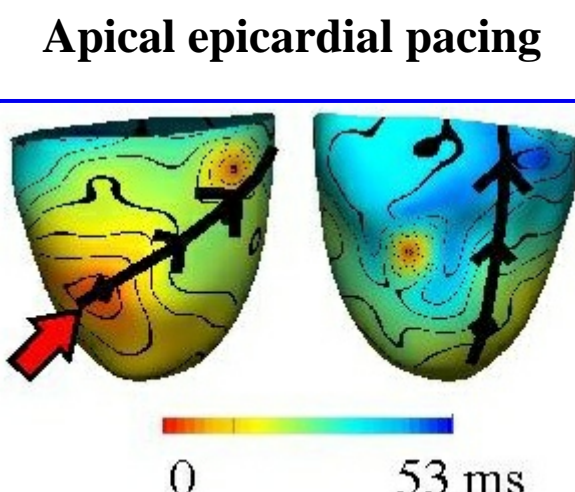


**Figure 4a:** The pacing site is represented by the red arrow. See Figure 2a legend and text for details.

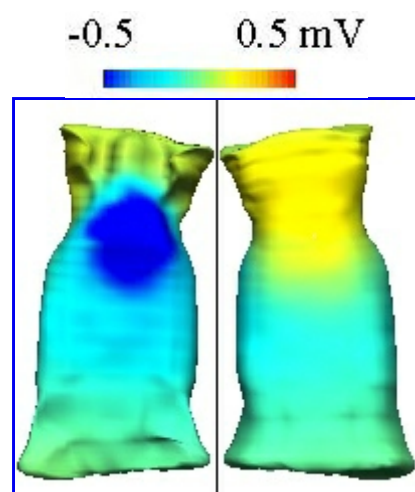


**Figure 4b:** See Figure 2b legend and text for details.

## Posterior epicardial pacing

Epicardial propagation during posterior-basal pacing was markedly slower in comparison to normal sinus rhythm, as illustrated in Figure 3a. The [animated activation sequence](#) also highlights this dramatic decrease in the speed of excitation propagation, which was likely to be due to a primarily circumferential spread of ventricular excitation following ventricular capture. Under these conditions, there were just two sites of epicardial activation breakthrough (one of which was the earliest site of activation, near the pacing site). This contrasted to the multiple breakthrough sites observed during normal sinus rhythm.

Alterations to the cardiac activation sequence were clearly reflected in changes to the BSPM, as shown in Figure 3b. The [BSPM animation](#) shows a reversal in the nature of the electropotential variations compared to normal sinus rhythm. Abnormal ventricular excitation resulted in a dramatically depressed ABP, as shown Figure 5.

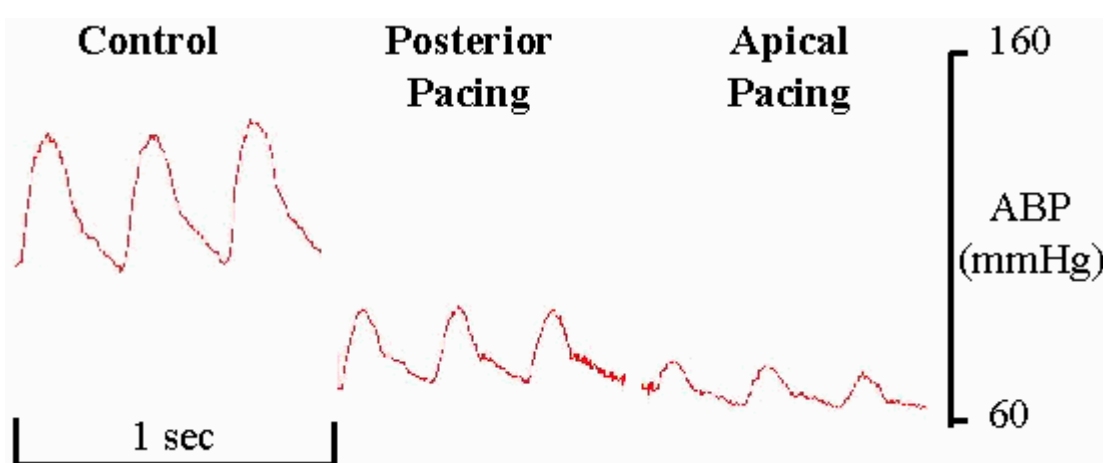


**Figure 5:** Arterial blood pressure (ABP) traces during normal sinus rhythm (Control) and epicardial pacing manoeuvres. Haemodynamics and electrical activity returned to control after pacing was stopped.

## Apical epicardial pacing

Apical pacing also dramatically decreased the speed of epicardial activation, as illustrated in Figure 4a and by the [animated activation sequence](#). Associated with this physiological intervention were corresponding changes in the BSPM (shown in Figure 4b and by the [BSPM animation](#)). The decrease in ABP compared to the control state (Figure 5) was similar for the two pacing interventions.

## Conclusions

We have established a computational and experimental framework to simultaneously record *in-vivo* body surface and epicardial potentials. We now aim to undertake a thorough validation study to investigate the suitability and accuracy of several ECG inverse approaches under normal and pathological conditions. This study will seek to determine the effects of geometry and individual variability by comparing the customised meshes with anatomically accurate meshes obtained from CT or MR. It will also seek to determine the level of accuracy with which electrocardiac events can be localised and the sensitivity of the predictions with respect to errors in geometric measurements and signal recordings. The information gained from this validation study will help to determine the feasibility of using an integrative computational inverse and body surface mapping approach as a clinical myocardial diagnostic tool.

## Acknowledgements

This work was funded by the [British Heart Foundation](#) and [Wellcome Trust](#), as part of the [Cardiac](#)

[Autonomic Control Research Group's](#) research programme. We also appreciate the support from the Oxford Supercomputing Centre of Oxford University. We would like to acknowledge the advice and expertise of Attila Kardos, Gerardo Sanchez-Ortiz and Jerome Declerck regarding the echocardiographic studies and analysis, and thank Chris Hirst and Vivienne Harris for their tireless technical support.

## References

- [1] Huiskamp, G. and Greensite, F., "A new method for myocardial activation imaging", IEEE Trans. Biomed. Eng., vol. 44, pp. 433-446, 1997.
- [2] Nash, M.P., Thornton, J.M., Sears, C.E., Varghese, A., O'Neill, M. and Paterson, D.J., "Ventricular activation during sympathetic imbalance and its computational reconstruction", J. Appl. Physiol., (in press), 2000.
- [3] Bradley, C.P., Pullan, A.J. and Hunter, P.J., "Geometric modelling of the human torso using cubic Hermite elements", Annals of Biomed. Eng., vol. 25, pp. 96-111, 1997
- [4] Cheng, L.K. and Pullan, A.J., "Towards non-invasive electrical heart imaging", in Proceedings of the First Joint Meeting of BMES and IEEE/EMBS, p. 57, Atlanta, GA, October 1999.
- [5] Pullan, A.J., Cheng, L.K., Nash, M.P., Bradley, C.P. and Paterson, D.J., "Non-invasive electrical imaging of the heart - theory and model development", Ann. Biomed. Eng. (submitted), 2000.



Journal of the International Society for Bioelectromagnetism